3D Coil Setup as a tool for MR sensor characterization

Mathieu Correia

Instituto Superior Técnico, Lisboa, Portugal

October 2021

Abstract

To this end, this present work consists in the fabrication of a 3D Helmholtz Coil parallelly with the assembling of a 3D Magnetometer. Furthermore, a collection of sensors was gathered to assess the functionality of our 3D Helmholtz Coil as a tool for sensor characterization and additionally, to be able to characterize our 3D Magnetometer in every sensitive axis.

All sensors were successfully characterized regarding, noise spectrum, detectivity, MR curve, noise, and low frequency AC magnetic field sensing. In addition, the coils were additionally tested as a tool for sensor linearization, by the application of a crossed DC magnetic field while being characterized regarding its MR curve.

Preface

This document was written and made publicly available as an institutional academic requirement and as a part of the evaluation of the MSc thesis in Bioengineering and Nanosystems of the author at Instituto Superior Técnico. The work described herein was performed at the INESC-MN institute of Instituto superior Técnico (Lisbon, Portugal), during the period September-October 2021, under the supervision of Prof. Susana Isabel Pinheiro de Cardoso Freitas.

Introduction

The data storage market was revolutionized by MR Sensors, which allowed the recording industry to display a substantial increase in storage density and data longevity [1]. MR sensors came to give attractive propositions to other fields of study, for instance, ABS sensors (automotive market) [2]. Moreover, the detection of low frequency alternate currents by MR Sensors has some interesting application in the field of human healthcare (20-300 Hz), geological investigation (0.01-5 Hz), and magnetic anomaly detection (0.04-2 Hz) [4]. Allied to the capability of being microfabricated at substantially high rates, MR sensors are optimal choices for several applications.

Tunnel Magnetoresistive sensors are one of the most forthcoming sensors in spintronics devices due to their high MR ratios, great detectivity in the low-frequency limit [3], and CMOS compatibility [5].

Currently, MR sensors, although capable of fulfilling a wide variety of demands, are limited to sensing a single component of an external magnetic field. Propositions with the complete 3D sensing integration lack compactness, sensitivity, and detectivity. This type of sensor with multiaxial sensing would substantially benefit industrial and biomedical diagnostic techniques for the robotic sensing industry, making the current investigation and research considerably beneficial. As a result of this vast potential, the INESC-MN spintronic department has been studying and investigating these types of MR sensors for a while now. This creates a need for a device that could accurately characterize a 3D Magnetometer in all sensing directions, such as, a portable setup of a 3D Helmholtz Coil.

In addition, this device could lead to some new types of sensor characterization being available at INESC-MN, such as, the effect of linearization of cross magnetic fields throughout MR sensors and the measurement of a sensor's capability on detecting low frequency AC magnetic fields.

1 Theoretical Background

1.1 Magnetoresistive Sensors

MR sensors core rises from the exploitation of the magnetic properties of ferromagnetic material. The ferromagnetic material can exhibit spontaneous magnetization, a net magnetic moment in the absence of an external magnetic field.

MR sensors are based on the MR effect that describes the change in the material's

electric resistance according to its magnetization, which can be changed with the assist of an external magnetic field.

They exhibit a maximum and a minimum magnetization, which in turn allows us to calculate the magnetoresistance of the device:

$$MR(\%) = \frac{Rmax - Rmin}{Rmin} * 100 \qquad (1)$$

There are three types of MR sensors, AMR, anisotropic magnetoresistance, GMR, giant magnetoresistance and TMR, Tunnel Magnetoresistance.

AMR is described by the change in electrical resistance regarding the orientation of the material's magnetization. For most materials, when current and magnetization are parallel (higher probability of electron scattering), we have a higher resistance than in the reverse situation.

GMR is quantum mechanical effect which finds that in layered magnetic structures, the resistivity depends on the relative alignment of the magnetizations of adjacent ferromagnetic layers. The stack consists in two ferromagnetic layers separated by a non-magnetic spacer, which creates a spin-polarizer effect, filtering electrons according to their spin, which creates a difference in electrical resistance according to the magnetization the ferromagnetic layers.

TMR is very similar with the GMR effect, the only difference is that instead of having a non-magnetic spacer, it has an insulator, that acts like a more efficient spin-filter, leading to a higher MR ratio. The interface phenomenon is called quantum tunneling, which is related with the overlap of the exponentially decaying wavefunction of the electron inside the barrier, which means that the current exponentially decreases with the increase in barrier thickness.

Spin-Valves are one of the most famous sensors that are based on the GMR effect. They consist in an antiferromagnetic layer adjacent to one of the ferromagnetic layers. This antiferromagnet goal is to pin the ferromagnetic magnetization to a fixed orientation magnetization, respectively, a fixed layer, to be used as a reference against a free-layer magnetization that is left free to be aligned with an externally applied field, which will allow the free layer to rotate between a parallel state and an antiparallel state relative to the magnetization of the fixed layer [6]. These two states, regarding electrical resistance, show a vast difference between them, providing an excellent readout of the magnetization state of the device.

Magnetic tunnel junctions are one of the most developed sensors based on the TMR effect. They are similar to spin-valves, but with an insulator barrier as described above, where the conduction is explained by to availability of empty states to receive spin down and spin up electrons, making parallel magnetizations more prone for electron conduction, therefore decreasing resistance.

1.2 Linear Magnetoresistive Sensors

The easiest way to measure the MR in an MR sensor is to measure the change in resistance plotted against an applied magnetic field.

The typical and desired MR curve for sensing applications is the one described below.

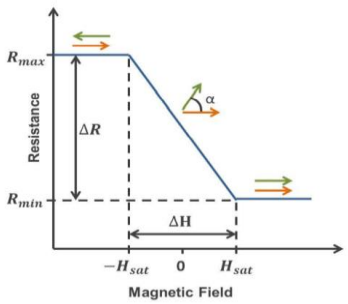

Figure 1 - Ideal MR Curve

Which possess a linear sensing range given by ΔH that translates into a resistance change given by ΔR.

The sensitivity of our sensor is dependent on the slope of our linear range, the bigger it is, more sensitive will be the resistance shift for a given magnetic field oscillation and is given by the following equation:

$$S\ sensor\ =\ MR\ /\ \Delta H\ [\%/Oe] \qquad (2)$$

1.3 Noise Sources in Magnetoresistive Sensors

There are several types of noise sources, such as:

1.3.1 Thermal Noise

Thermal noise exists in any type of electrical device and is caused by a random thermal motion of electrons and is directly proportional to temperature.

1.3.2 Shot Noise

Shot Noise is related to current that flows through discontinuities in a circuit when all outside noise sources are removed, such as, the interface barrier in MTJ's.

1.3.3 Random Telegraph Noise

Oxygen vacancies in the tunnel barrier cause random telegraph noise in magnetic tunnel junctions. These vacancies can enclosure an electron, increasing the resistance of the device. When the system returns to the ground state, the electron is released, causing the system to decrease the resistance back to the original value.

1.3.4 1/f noise

This noise exists practically everywhere in nature and is usually related to charge trapping in crystal defects. There are two sources of 1/f noise, magnetic 1/f noise and electronic 1/f noise.

Electronic 1/f noise is usually associated with charge trapping in interface barriers caused by defects in these barriers, with the random liberation of this electron following a probability amplitude that favors energy concentration at low frequencies.

The magnetic 1/f noise can be described by the magnetization switching of our ferromagnetic layers at the interface between our free and pinned layers [7] [8]. This magnetic 1/f noise is also inversely proportional to the frequency. A frequency marks the threshold where the 1/f noise is lower than all other noise types; that is called the 1/f knee.

1.4 Detectivity

Detectivity is defined by the slightest change in magnetic field that our sensor can detect for a particular frequency and applied field. This means that the sensor does not recognize any change below that value of magnetic field variation due to the total noise level overlap on our signal output.

Detectivity can be expressed by the output noise of the sensor divided by the sensor sensitivity.

$$D = \frac{S_V}{\Delta V / \Delta H} \left[\frac{T}{\frac{1}{Hz^{\frac{1}{2}}}}\right] \quad (4)$$

1.5 Helmholtz Coils

The ability to produce arbitrary magnetic fields has always been a targeted ability ranging from magnetic resonance imaging to ambient magnetic field cancellation, hall sensors calibration, and magnetometer characterization. Some of these applications require a spatially uniform multiaxial magnetic field. To this end, the Helmholtz coil is a device that creates a highly uniform magnetic field consisting of two electromagnets on the same axis. A Helmholtz Coil consists of a paired arrangement of identical circular solenoids mounted coaxially at one coil radius from each other.

The following equation provides the magnetic field generated in the center of the Helmholtz coil,

$$B = \left(\frac{4}{5}\right)^{3/2} \frac{\mu_0 n I}{R} \quad (5)$$

Where R is the coil radius, I is the coil current, x is the coil distance on-axis, μ_0 is the permeability constant and n is the number of turns per coil.

2 3D Helmholtz Coil Fabrication

To design the respective 3D Helmholtz coil, an open-source python library was used, magpylib. This python library is used for calculating magnetic fields, currents and provides the necessary tools to generate, manipulate and visualize assemblies of magnetic sources.

Using this library, a script was developed to calculate the necessary coil parameters to obtain the desired requirements for our setup. Such parameters consist in, maximum size, minimum magnetic field, wire diameter and number of turns per layer.

The output parameters were the coil diameter, internal distance between coils, coil width, coil height, coil resistance, coil power dissipation and necessary wire to construct the coil, for each axis.

Some simulations were then did, to validate the uniformity of the Magnetic Field in the center of each axis.To fabricate the model, a 3D modeling software named SolidWorks was used. The geometric model of our 3D Helmholtz Coil is based on the previously obtained parameters by our simulator. The model was designed to align perfectly our coils in each specific axis, which led to the assembling of every coil integrated into a single modeling part. This was later exported, saved, and introduced into the software of the INESC-MN 3D printer, which

printed the device using PVA. Here follows the result of the coil setup:

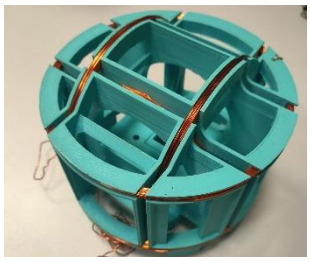

Figure 1 - 3D Helmholtz Coil Setup

2.1 3D Helmholtz Coil Calibration

Proceeding to setup calibration, a bipolar operational amplifier called kepco bop bib488.2 was used, to supply current to the 140 Oe setup and consequently, to power this setup. In addition, we used a gaussmeter to measure the magnetic field generated in the geometric center of our coil. This yielded three calibration curves that were matched against the magnetic field theoretical values calculated for each current input.

In general, the values presented a very low disparity. Despite this, the encountered difference between the calculated and experimental values is most likely due to the magnetization of surrounding metals. Also, the theoretical values did not took into account the earth's magnetic field.

3 Assembly of Magnetoresistive Sensors and Characterization

Since size was one of the primary focuses, the chip carrier we chose needed to be large enough to allow sensor manipulation but small enough to possess a particular competitive advantage. The chip carrier chosen was a Quad Flat No Leads (QFN) with electrical connections on the bottom of the carrier. To establish the contacts in our carriers, we needed a solution that could allow the facile replacement of the carrier by another carrier with different sensors since this work aims to allow the characterization of several low field sensors. To this end, we coupled our carrier with an open-top socket to acquire the sensor's signal where the carrier could be easily removed and substituted by another. Meanwhile, a PCB (5x5cm) was designed to establish the breakout from the socket to 4 arrays of 10 pins on each side of our PCB.

3.1 Sensor Assembly

Several specific sensors were assembled to allow to understand how reliable and prone the 3D Coil setup regarding sensor characterization was.

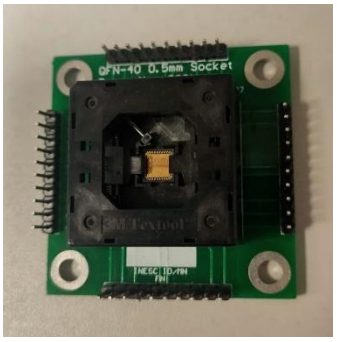

Figure 2 - Graphical representation of final assembled device, socket + PCB

3.1.1 3D Magnetometer from array of Magnetic Tunnel Junctions of AlOx

Ultimately, the final goal of this sensor is based on the ability to measure 3D magnetic fields while maintaining a compact size device. Therefore, this would require some planning regarding the disposition of the sensor. One of the possibilities was incorporating a vertical PCB with a sensor consisting in an array of MTJ's, from Mafalda Veiga Thesis, to define our Z-axis. On the other hand, this would not be a very compact solution. Since the vertical PCB was not an option, we tried to integrate the MTJ array vertically, right on top of the chip carrier.

This attempt to rotate our sensor ninety degrees in the longitudinal axis was time-consuming because it required a wire bounding in two orthogonal planes instead of just one, which is the case of regular wire bonding. The wire bonding machine existing at INESC does not rotate the stage out-of-plane, which means that to proceed to the wire bonding, the sensor would need to be rotated after the wire bound on the sensor contact pads. This is a tricky maneuver to attempt without breaking the wire. In addition, the pads were passivated with Ta, which with the wire material and needle size, difficulted the attachment of the wire to the contacts.

To procedure started with the wire bound in the sensor pads, with the sensor horizontally placed on top of our carrier, and leave a certain amount of loose wire, not establishing the second bound on the chip carrier. Then, very carefully, rotating and

gluing the sensor to afterward push the loose end of the wire into the chip carrier contacts, establishing then the second bounding.

3.1.2 Two sensors provided by INESC-MN

Two types of TMR sensors were provided by INESC-MN, from one of the Multiproject Wafer run (MPW run #11) from a 200mm diameter wafer.

For readability purposes we will call them respectively, MTJ 1 and MTJ 2, for the (680 um x 400um) chip and the (300um x 420um) chip.

The incorporation of these sensors into our chip carrier was done by normal wire-bounding onto our QFN.

3.1.3 Spin-Valve with and without Flux concentrator

For last, two spin-valves sensors were used with the same characteristics except for, in one of the sensors, the incorporation of a flux concentrator in the silicon substrate.

The flux concentrator objective in this sensor is to deviate the magnetic flux lines of other sensitive directions into the sensor's sensible direction. These sensors were built and characterized to determine the main noticeable differences between both sensors' sensitivity, detectivity, coercivity, and linear response.

The incorporation of these sensors into our chip carrier was done by normal wire-bounding onto our QFN.

3.2 Sensor Magnetoresistive Curve

3.2.2 Acquisition Software and Electronics

To acquire the MR curve from our 3D sensor, the 3D Helmholtz coil was used. To that end, a script was elaborated in Visual Studio under the programming language C#.

The script used the calibration curves for each Helmholtz Coil axis to transform every current input received by our coils into the respective value of the applied magnetic field. Meanwhile, we collected the voltage at the sensor terminals using a two-probe method, which applies a constant current, Ibias, in the outer sensor's contact's while measuring the voltage simultaneously. By using Ohm's law, V = RI, we can easily calculate the sensor's resistance, hence, plotting our MR curve.

All the devices, as for, Voltmeter and both current sources, Coils, and Ibias, were all connected to GPIB that for himself, connects to the computer, where the proper software was installed to be able to run the C# script on Visual Studio.

The input parameters are the desired axis in the 3D Coil setup, the desired number of measurements and the interval between them.

3.3 Sensor's Characterization

3.3.1 Magnetoresistive Curve Characterization

3.3.1.1 Magnetoresistive Curve for our 3D magnetometer

The sensor was successfully characterized regarding his MR curve. As the linear range presented by our sensors is in the order of -50, 50 Oe, the entire linear range could not be characterized through the 3D coils setup due to the coil's small size, leading to a considerable power dissipation for currents above 3.5 Amperes.

Here follows the MR characterization of the partial linear range for X, Y and Z-Axes.

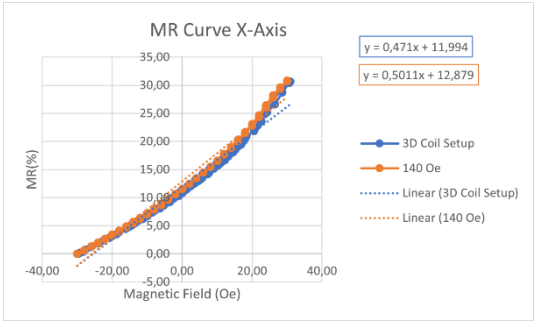

Figure 3 - Linear range of magnetoresistive curve for the X-Axis

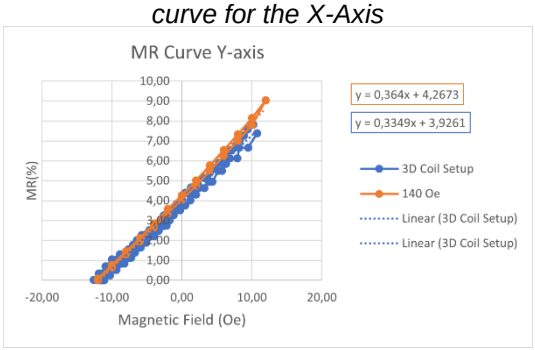

Figure 4 - Linear range of magnetoresistive curve for the Y-Axis

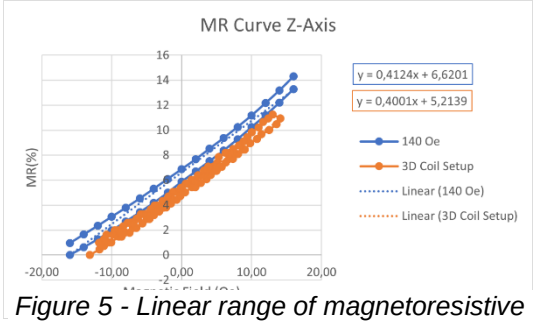

Figure 5 - Linear range of magnetoresistive curve for the Z-Axis

From the given plots, we can notice a close similarity between the tendency line from the linear range MR curves of both setups. By comparing for each direction, the slopes of the linear sensing area, we get a 6% (X-Axis), 8% (Y-Axis), and 3% (Z-Axis) difference from the reference's values of the 140 Oe setup.

The obtained difference is believed to be led by geometrical imprecision, which could be improved if we build another structure integrated into the 3D Coil Setup that would lock the chip carrier in the geometrical center of the coils. One other possible explanation could be the number of voltages reading averages measures of our sensor by the 140 Oe Setup. In our script, the voltage was directly read from the voltmeter, without measured averages, leading to some data disparity.

3.3.1.2 Magnetoresistive Curve for MTJ 1 and MTJ 2

The sensors were successfully characterized regarding their MR curve.

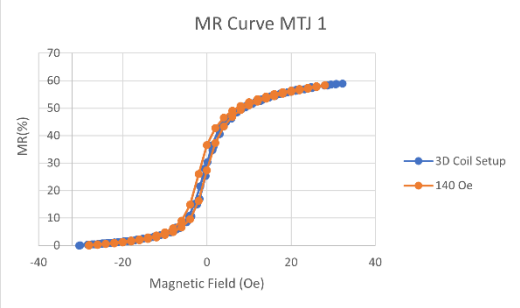

Figure 6 - Magnetoresistive curve characterization of MTJ 1

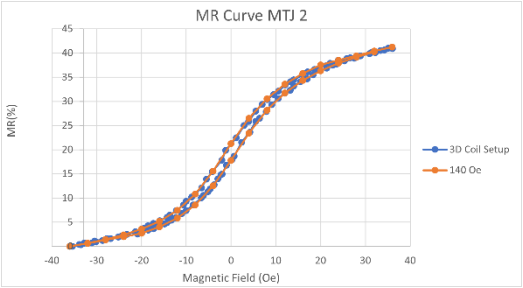

Figure 7 - Magnetoresistive curve characterization of MTJ 2

Both sensors present a very similar behavior in our measured setups, presenting a percentual MR difference of 1% for MTJ 1 and MTJ 2.

3.3.1.3 Magnetoresistive Curve for Spin-Valve Sensors

MR spin-valves are often coupled with flux concentrators due to their magnetic flux increases through the Spin-Valve sensing direction. This will theoretically lead to an increase in the sensitivity of our sensor if the magnetic flux is correctly shifted.

The sensors were successfully characterized regarding their MR curve.

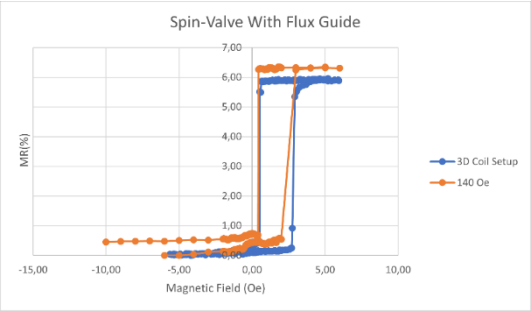

Figure 8 - Magnetoresistive Curve for Spin-Valve with Flux Guide

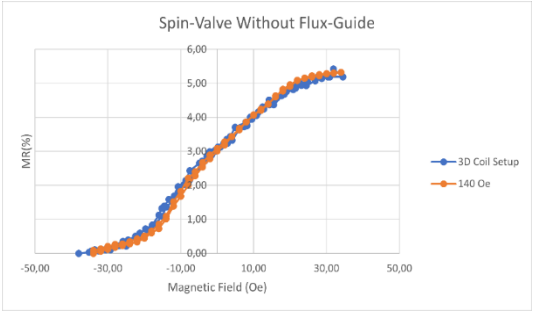

Figure 9 - Magnetoresistive Curve for Spin-Valve without Flux Guide

Both sensors present a very similar behavior in our measured setups, presenting a MR difference for our Flux concentrator and No Flux concentrator sensor of 6.5% and 2.4%, respectively. The stepper and more sensitive response in the 3D Coil Setup were linked to how the measurement was done in the 140 Oe setup, with a more significant magnetic field disparity between the points in the critical sensing area.

As expected, we see an increase in the sensitivity of our sensor of about 400 times the value of our spin-valve without the flux concentrator.

In general, the MR curve for both sensors measured in two different setups was very approximated with some room for improvement, such as, precise geometrical alignment of the sensor in both correspondent setups.

3.3.2 Noise level and Detectivity Results

3.3.2.1 Noise level and Detectivity Results for 3D magnetometer

Bellow follows the noise spectrum and detectivity table measurements from our 3D magnetometer.

Table 1 - Noise 3D Magnetometer Specific Data

	X-axis	Y-Axis	Z-Axis
Rsensor (KOhm)	139	276	182
Rpotentiometer (KOhm)	20	20	20
Vbias (Volt)	1.38	1.4	1.5
TMR (%)	40.22	39.80	40.33
Detectivity (nT/√Hz) @30 Hz	7.03	6.57	7.11
Detectivity (nT/√Hz) @1 kHz	1.31	3.43	1.17

In the low-frequency regime, we can see that we have a similar minimum detectable magnetic field variation. Detectivity levels vary from 6.57 nT/√Hz to 7.11 nT/√Hz, at 30 Hz, for the Y and Z directions, respectively. This is a good outcome to validate this 3D magnetometer regarding its 3D sensing ability, allowing every axis to be in the same range of detectability, which gives no differential magnetic sensing ability for the magnetometer and improved full axes coherency

3.3.2.2 Noise level and Detectivity Results for MTJ 1 and MTJ 2

Bellow follows the noise spectrum and detectivity table measurements of MTJ 1 and MTJ 2.

Table 2 - Noise MTJ's Specific Data

	MTJ 2	MTJ 1
Rsensor (KOhm)	1673	811
Rpotentiometer (KOhm)	20	20
Vbias (Volt)	1.48	1.35
TMR (%)	59.61	76.38
Detectivity (nT/√Hz) @30Hz	22.01	9.86
Detectivity (nT/√Hz) @1 kHz	5.34	2.19

We obtained the following detectivity levels in the low-frequency regime, 9.86 nT/√Hz and 22.01 nT/√Hz, at 30 Hz for our MTJ 1 and MTJ 2, respectively.

3.3.2.3 Noise level and Detectivity Results for Spin-Valve Sensors

Magnetic tunnel junctions present, in a typical situation, a considerably higher MR ratio than in Spin-Valves, but this comes with a cost of increased intrinsic noise. MTJ offers a great possible alternative to spin-valves if their signal-to-noise ratio surpasses those of spin-valves. The fact that MTJ possesses a higher intrinsic noise is due to several reasons. For instance, above the 1/f knee, one primary source of noise that is present in MR devices is thermal noise. In addition, shot noise becomes a critical key factor in MTJ devices due to the discontinuity in the conduction medium that the MTJ barrier represents. In the low-frequency regime, we also have a more significant contribution of 1/f noise than in spin-valves.

In some cases, it can even reach a Hooge parameter 300 times bigger than in spin-valves [9].

Here follows a table with our given values for potentiometer resistance, sensor resistance, bias voltage, and MR and a brief sum-up of the detectivity plots.

Table 3 - Noise Spin-Valve Specific Data

	Flux concentrator	N/Flux concentrator
R sensor (Ohm)	309	447
R potentiometer (Ohm)	512	506
Vbias (Volt)	0.51	0.63
MR (%)	6.53	6.68
Detectivity (uT/√Hz) @30Hz	0.32	1.46
Detectivity (nT/√Hz) @1 kHz	43.94	217.62

In these Spin-Valves sensors, we can see that the intrinsic sensor noise is similar to our MTJ sensors, which gives our MTJ a significant competitive advantage regarding detectivity that is enhanced because of MTJ's naturally more considerable sensitivity.

In addition, we can notice a lower Flux concentrator sensor noise compared with the standard spin-valve sensor. This will, in turn, with a more sensitive slope, lead to a detectivity in our Flux concentrator sensor 4,5 times lower than the detectivity of our normal spin-valve, in the low-frequency regime, at 30Hz.

Conclusion

Additionally, the characteristics of the MR sensors competing technology for ultra-low field detection has come a long way. From fabrication of single MTJ's, with detectivities ranging from 350 nT/√Hz at 1 Hz with a 3.3%/Oe sensitivity, to MTJ arrays with more than 1000 junctions, achieving detectivities of 16.2 nT/√Hz at 1 Hz and TMR ratios of 63% [1] [2]. Given all these new advances on MR sensors for low field detection, our 3D Magnetometer, composed of a Wheatstone bridge of MTJ's array, with a detectivity at 30 Hz of 7.03, 6.57 and 7.11 nT/√Hz, for the X, Y, and Z-Axis has preeminent abilities. In addition, we obtained a TMR of 59.61% and 76.38%, with a detectivity at 10 Hz of 22.01 nT/√Hz and 9.86 nT/√Hz and a sensitivity of 4.58%/Oe and 1.29%/Oe, for MTJ 2 and MTJ 1, respectively.

Both sensors, 3D Magnetometer and MTJ 1 and MTJ 2, present a good competitive profile for low field measurement sensors. Despite this, the measured spin-valves had an intrinsic noise level very similar to the MTJ measured, which did not give rise to a prominent device for low field measurement.

If the 3D Magnetometer were to be rebuilt, we would use the MTJ 1 due to the smaller magnetic linear range, which our sensor can fully characterize, presenting the second smallest detectivity range with the highest MR.

4 AC magnetic sweep

To test our sensor ability to sense a low-frequency AC magnetic field, we had to create an oscillating magnetic field in our 3D Helmholtz coil and do a magnetic and frequency sweep through our sensor. We assessed its capability to detect a low-frequency magnetic field by calculating the measured sensor response's SNR ratio (Speak/Sbackground). The background is the sensor signal noise limit of field detectivity, given by SNR = 1. This type of experiment is elucidating to better understand the limitations in our sensor's magnetic sensing. More fit and real data can be obtained from the sensors output subjected to a low AC magnetic field due to the actual presence of the magnetic field, and not only the theoretical estimation of it. To generate the oscillating magnetic field, we used our 3D Coil Setup, respectively, the X-Axis. The frequency sweep was done from 0 to 100Hz, with the established AC magnetic fields oscillating at a frequency of 10, 20, 40, and 80 Hz.

Both sensors and 3D Coil Setup are inside a magnetically shielded box. The Helmholtz coil was connected to a function generator, and the data was interpreted using the noise setup. For each measurement, 1000 averages were calculated with an RBW of 1.

4.1 Minimum detectable field for the X-Axis of our 3D Magnetometer

The following plots were obtained for each of the measured frequencies. Voltages peaks can be observed from our sensor's output where the AC magnetic field was applied.

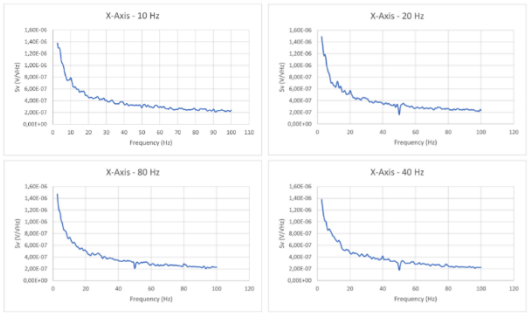

Figure 10 - AC magnetic field detectivity for low field frequency, respectively, 10, 20, 40 and 80 Hz of X-Axis of 3D magnetometer

The estimated root means square value for the measured frequencies, 10, 20, 40, and 80 Hz, is 9.27, 8.85, 5.60, and 3.36 nT for an SNR of 1.

4.2 Minimum detectable field for MTJ 1 and MTJ 2

The following plots were obtained for each of the measured frequencies. Voltages peaks can be observed from our sensor's output where the AC magnetic field was applied.

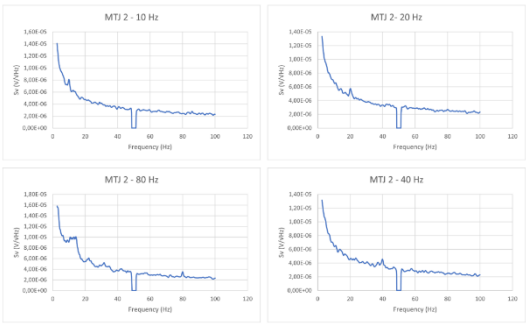

Figure 11 - AC magnetic field detectivity for low field frequency, respectively, 10, 20, 40 and 80 Hz of MTJ 2

The estimated root means square value for the measured frequencies, 10, 20, 40, and 80 Hz, is respectively, 43.06, 25.74, 23.90, and 16.50 nT for an SNR of 1.

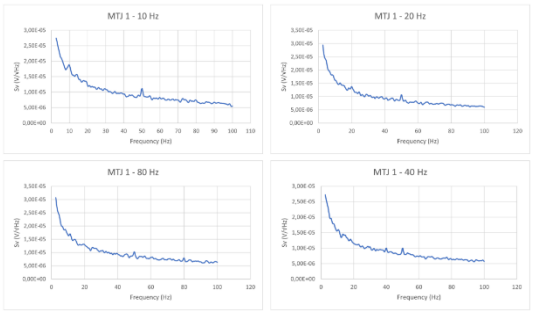

Figure 12 - AC magnetic field detectivity for low field frequency, respectively, 10, 20, 40 and 80 Hz of MTJ 1

The estimated root means square value for the measured frequencies, 10, 20, 40, and 80 Hz, is 21.94, 18.36, 17.22, and 13.66 nT for an SNR of 1.

4.3 Minimum detectable field for Spin-Valve Sensors

The following plots were obtained for each of the measured frequencies. Voltages peaks can be observed from our sensor's output where the AC magnetic field was applied.

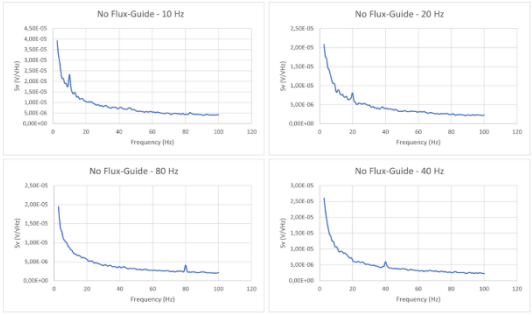

Figure 13 - AC magnetic field detectivity for low field frequency, respectively, 10, 20, 40 and 80 Hz of Spin-Valve without Flux-Guide

The estimated root means square value for the measured frequencies, 10, 20, 40, and 80 Hz is respectively, 87.13, 66.92, 46.22, and 33.18 uT for an SNR of 1.

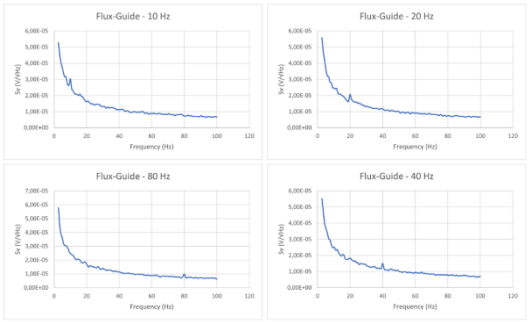

Figure 14 - AC magnetic field detectivity for low field frequency, respectively, 10, 20, 40 and 80 Hz of Spin-Valve with Flux-Guide

The estimated root means square value for the measured frequencies, 10, 20, 40, and 80 Hz, is 76.28, 43.16, 33.25, and 21.40 uT for an SNR of 1

Conclusion

All our sensors could detect a low-frequency magnetic field and were characterized regarding detectivity limits in the low-frequency field compartment, providing an excellent readout of the sensor's detective capacity and consequently increasing our sensor's panorama comprehension.

We can see that, except for the X-Axis sensor, all the other values were above the minimum detectable magnetic field oscillation. That is one of the key factors of having this type of sensor characterization, leading to more accurate data that can better define our sensing device.

In addition, the spin-valve sensors were the ones that had the biggest disparity between theoretical detectivity limitations and actual calculated values, having a minimum detectivity 172 and 46 times bigger than the expected one, for Spin-Valve with and without Flux-Concentrator, respectively.

The difference in these values is mainly related to applying an external magnetic field that will shift and generate more magnetic 1/f noise. Another reason was that the Vbias introduced into our sensors was not the same from this and the previous

measurements at 0 Tesla, changing the sensitivity and consequently the detectivity. This happened because of a problem in the potentiometer from the noise Setup, which disabled us from having the same consistent Vbias.

5 Flux concentrator MR Characterization with cross-field

5.1 Linearization Strategy

To promote sensor linearization, several techniques can be employed. One of them can be to apply an external permanent magnetic field in the transversal sensing direction. For this purpose, we used our 3D Coil Setup to measure the MR curve of our sensor with its easy axis in the X-axis and applied the external magnetic field in the Y-direction.

The following plots were obtained:

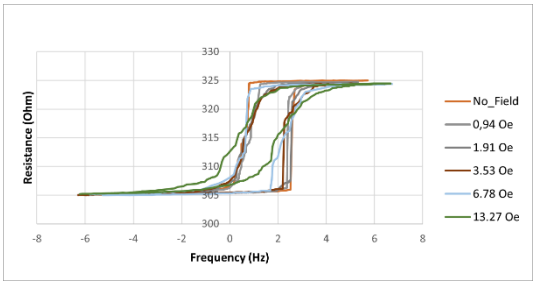

Figure 15 - Effect of crossed applied magnetic field on magnetoresistive curve of the Spin-Valve with Flux-Guide sensor

We can see a shift towards sensor linearization, with a decrease in the hysteric curve and sensitivity. The coercivity in the final MR measurement, 13.28 Oe, had a 30% reduction, a considerable coercive loss from 1.92 Oe to 1.36 Oe. In addition, the sensitivity had a reduction of 93%, going from a very steep linear range to a softer curve.

Conclusion

In conclusion, a compact, sensitive, and accurate 3D Coil Setup was built and provided several characterization measurements of a set of MR sensors.

We were able to measure the critical detectivity limit for our sensors; the Flux concentrator sensor detected an AC magnetic field of 88.48 uT; the non-flux concentrator 115.01 uT; both MTJ sensors provided by INESC-MN 48,66 nT and 22,38 nT, for MTJ 2 and MTJ 1; The X-Axis of our 3D magnetometer, 9.73 nT, all of them at 10 Hz.

Additionally, we were able to get, from a 0 Oe first measurement to an applied 13.2 Oe of crossed magnetic field, we observed a decrease of 30% and 93% in coercivity and sensitivity, respectively. Concluding that, this type of strategy has beneficial implications in MR sensors linearization strategies.

With this, we conclude that the 3D Coil Setup has showed to have good outcomes regarding sensor characterization, that broadens our sensor panorama comprehension.

Bibliografia

[1] C. H. Bajorek, "Magnetoresistive (MR) Heads and the Earliest MR Head-Based Disk Drives: Sawmill and Corsair," *Storage Special Interest Group,* p. 10, 29 05 2015.

[2] K. P. Gokhale..US Patente 4,835,467, 1989.

[3] J. Valadeiro, "Magnetoresistive sensors with pico-tesla sensitivities," . *Master's thesis, Instituto Superior Tecnico,* 2014.

[4] M. P. J. H. S. L. D. C. W. T. K. S. Q. D. Y. W. L. P. W. Z. Q. Z. P. L. J. P. W. Q. a. J. Z. Jinghua Hu, "Resolution improvement of low frequency AC magnetic field modulated MR sensors," *REVIEW OF SCIENTIFIC INSTRUMENTS,* vol. 88, p. 095006 , 2017.

[5] S.-J. Han1, "CMOS Integrated DNA Microarray Based on GMR Sensors," *Stanford University,* 2007.

[6] R. Waser, Nanoelectronics and Information Technology: Advanced Electronic Materials and Novel, Germany, 2012.

[7] X. L. B. S. a. G. X. C. Ren, "Low-frequency magnetic noise in magnetic tunnel junctions.," *Physical Review ,* vol. 69, nº 10, p. 104405, 2004.

[8] R. F. S. C. a. F. C. P. Freitas, "Magnetoresistive sensors," *Journal of Physics: Condensed Matter,* vol. 19, nº 16, p. 165221, 2007.

[9] H. B. A. S. K. P. J. Z. S. L. W. R. C. A. F. B. A. B.-H. R. W. a. D. S. erbert Weitensfelder, "omparison of Sensitivity and Low Frequency Noise Contributions in GMR and TMR Spin Valve Sensors with a Vortex State Free Layer," *Phys. Rev.,* vol. 10, nº 5, p. 054056, 2018.

[10] R. A. M. A. Ferreira, "Ion Beam Deposited Magnetic Spin Tunnel Junctions targeting HDD Read Heads, Non-volatile Memories and Magnetic Field Sensor Applications," *PhD thesis,* 2008.